IIETA International Information and Engineering Technology Association
Advancing the World of Information and Engineering

Journal Européen des Systèmes Automatisés
Vol. 59, No. 5, May, 2026, pp. 1477-1487
Journal homepage: http://iieta.org/journals/jesa

Algebraic Observer-Based Fault Diagnosis for Proton Exchange Membrane Fuel Cell Air Supply Systems with Sliding-Mode Derivative Estimation

Asma Rahmani*, Benalia Atallah, Bougrine Mohamed, Seghir Mohammed

LACoSERE Laboratory, Electrical Engineering Department, University of Amar Telidji, Laghouat 03000, Algeria

Corresponding Author Email: asma.rahmani@lagh-univ.dz

https://doi.org/10.18280/jesa.590523

Received: 8 March 2026
Revised: 4 May 2026
Accepted: 11 May 2026
Available online: 31 May 2026

Keywords:
proton exchange membrane fuel cell, air supply system, fault diagnosis, algebraic observers, finite-time reconstruction, robust exact differentiation

ABSTRACT

This paper presents a finite-time fault reconstruction strategy for proton exchange membrane fuel cell (PEMFC) air feed systems. The strategy combines algebraic methods with a robust exact differentiator. The proposed approach enables the reconstruction of both actuator and process faults using only measurable signals and their derivatives, without requiring full state observers. First, an algebraic framework is derived to express the system states and fault variables as functions of the measured outputs and a finite number of their time derivatives. Then, a robust exact differentiator is employed to estimate the required derivatives in finite-time under bounded perturbations, ensuring the convergence properties of the accurate fault reconstruction. The proposed approach offers a simple structure, reduced computational complexity, and ease of implementation due to its single-parameter tuning design. Simulation results obtained on a nonlinear PEMFC air-supply model under stepwise load-current variations from 150 A to 300 A and different simultaneous fault scenarios demonstrate fast convergence, accurate fault estimation, and robustness under noisy operating conditions. The proposed method achieves settling times below 0.3 s for both leakage and actuator faults, with low settling reconstruction errors and strong robustness against measurement noise. Comparative performance metrics with a super-twisting sliding mode observer are also provided.

1. INTRODUCTION

Proton exchange membrane fuel cells (PEMFCs) have gained considerable attention as clean power sources for both automotive and stationary applications, due to their high energy conversion efficiency, fast dynamic response, and negligible local pollutant emissions [1, 2]. The air supply subsystem constitutes a critical component of the PEMFC power plant, since it governs oxygen delivery to the cathode and directly influences the oxygen excess ratio, stack voltage, and overall system efficiency. Insufficient air supply can lead to cathode oxygen starvation, which accelerates membrane degradation and shortens the fuel cell lifetime [3].

Reliable fault detection and isolation in the air path is therefore of practical importance for safe and efficient PEMFC operation. In the recent literature, three main families of fault diagnosis approaches have been developed and evaluated for PEMFC systems. Data-driven methods include neural networks, support vector machines, and deep learning architectures. They show promising classification performance using electrochemical impedance spectroscopy (EIS) data or voltage/current measurements without a physical model [4-6]. However, these methods typically require large labelled training datasets, suffer from limited generalization over different stacks and operating conditions, and offer only limited physical insight into the diagnosed faults.

Model-based fault diagnosis methods exploit the physics-based dynamics to generate fault-sensitive information, making them effective for PEMFC air supply problems [7, 8]. Among the model-based strategies, observer-based approaches are particularly interesting since they can reconstruct unmeasured internal states and estimate fault signals in real time [9]. In the PEMFC context, various observer architectures have been studied, including adaptive Kalman filters [10] and linear parameter-varying (LPV) observers [11]. While these methods provide valuable diagnostic information, they typically rely on asymptotic convergence, meaning that the fault estimate improves gradually over time and may respond slowly during rapid transients, and often require residual evaluation with manually tuned detection thresholds. More recently, Yang et al. [12] proposed an augmented LPV observer that simultaneously reconstructs component faults and performs active fault-tolerant control of the oxygen excess ratio in the PEMFC air management system. In the domain of finite-time and sliding-mode approaches, Guo et al. [13] introduced an adaptive prescribed-performance controller that handles unknown air compressor faults, while Wang et al. [14, 15] developed fixed-time and finite-time sliding-mode fault-tolerant control frameworks for the supply manifold and compressor subsystems.

Another possible approach is to use algebraic observer techniques, based on the differential-algebraic framework of

Diop and Fliess [16] and Fliess and Sira-Ramirez [17]. In this approach, system states and fault signals are expressed as functions of the measured outputs and their time derivatives. This eliminates the need for asymptotic convergence and yields fault estimates that are available as soon as accurate derivative information is obtained. Algebraic observers have been applied to PEMFC systems by Baroud et al. [18, 19], who demonstrated finite-time state estimation and also combined algebraic observers with output-feedback control. Jing et al. [20] proposed multi-objective sliding-mode control with adaptive algebraic observers, while Liu et al. [21] developed a robust model-based fault diagnosis scheme for the PEMFC air-feed system. Building on such algebraic frameworks, Flores-Mendez et al. [22] combined algebraic identification with extended state observers to improve the robustness of fault diagnosis in nonlinear systems, demonstrating non-asymptotic fault estimation under realistic perturbation levels.

A common practical challenge when using algebraic methods is the sensitivity of numerical differentiation to measurement noise. Direct finite-difference approximations lead to the amplification of high-frequency disturbances and compromise the quality of the reconstructed signals. To address this issue, Levant introduced higher order sliding mode (HOSM) differentiators [23, 24], which provide exact derivative estimation in finite-time for signals with bounded higher-order derivatives. The theoretical properties of these differentiators have been rigorously established through strict Lyapunov functions by Moreno and Osorio [25].

The present work combines the direct algebraic fault reconstruction framework with a robust exact differentiator based on the second-order sliding-mode algorithm. The differentiator is parameterized so that only a single design parameter an upper bound on the second derivative of the measured signal requires tuning. The diagnosis focuses on actuator faults (compressor motor degradation) and process faults (supply manifold leakage), which represent the most common failure modes in the air supply subsystem. Unlike observer-based approaches that achieve fault estimation only asymptotically, the proposed algebraic framework yields fault reconstruction formulas that are instantaneous functions of measured signals and their derivatives. Combined with the finite-time convergence of the robust exact differentiator, this results in a fault diagnosis scheme that achieves finite-time reconstruction with a guaranteed finite settling time.

The remainder of this paper is organized as follows. Section 2 describes the PEMFC air supply system model and the fault parameterization. Section 3 develops the algebraic observability analysis and the direct fault reconstruction formulas with explicit robustness considerations. Section 4 presents the robust exact differentiator and its application to the PEMFC diagnosis problem. Section 5 presents simulation results using the Pukrushpan PEMFC model. And Section 6 concludes the paper.

2. PROTON EXCHANGE MEMBRANE FUEL CELL AIR SUPPLY SYSTEM MODELING

2.1 System description

The PEMFC air supply subsystem comprises a centrifugal compressor driven by an electric motor, a supply manifold, and the fuel cell stack cathode. Ambient air is drawn by the compressor and delivered through the supply manifold to the cathode inlet, where oxygen participates in the electrochemical reaction. The cathode outlet is connected to the exhaust through a back-pressure orifice. The schematic of the PEMFC air-feed system is shown in Figure 1.

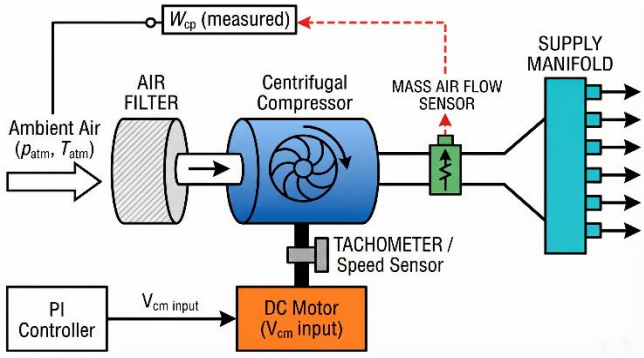

Figure 1. Proton exchange membrane fuel cell (PEMFC) air feed system scheme

The primary control objective is to regulate the oxygen excess ratio λ_{O_2} around the optimal value of 2, which balances oxygen availability against parasitic compressor power consumption [26, 27]. The oxygen excess ratio is defined as:

$$\lambda_{O_2} = \frac{W_{O_2,in}}{W_{O_2,rct}} = \gamma_{18}(P_{sm} - P_{ca}) / (\gamma_{19} I_{st}) \tag{1}$$

where, $W_{O_2,in}$ is the inlet oxygen mass flow, $W_{O_2,rct}$ is the reacting oxygen flow, p_{sm} is the supply manifold pressure, p_{ca} is the cathode pressure, and I_{st} is the stack current.

2.2 Fourth-order dynamic model

A control-oriented fourth-order model derived from mass and energy balance principles is adopted [26]. The state vector is:

$$x = [P_{O_2} \; P_{N_2} \; \omega_{cp} \; P_{sm}]^{\mathrm{T}} \tag{2}$$

where, p_{O_2} and p_{N_2} are the oxygen and nitrogen partial pressures in the cathode, and ω_{cp} is the compressor angular velocity. The nominal system dynamics are:

$$\dot{P}_{O_2} = \gamma_1(P_{sm} - P_{ca}) - \gamma_3 P_{O_2} W_{ca,out} / (\gamma_4 P_{O_2} + \gamma_5 P_{N_2} + \gamma_6) - \gamma_7 I_{st} \tag{3}$$

$$\dot{P}_{N_2} = \gamma_8(P_{sm} - P_{ca} - \gamma_3 P_{N_2} W_{ca,out} / (\gamma_4 P_{O_2} + \gamma_5 P_{N_2} + \gamma_6) \tag{4}$$

$$\dot{\omega}_{cp} = -\gamma_9 \omega_{cp} - \left(\frac{\gamma_{10}}{\omega_{cp}}\right) \Psi W_{cp} + \gamma_{13} V_{cm} \tag{5}$$

$$\dot{P}_{sm} = \gamma_{14}[1 + \gamma_{15}\Psi]\left(W_{cp} - \gamma_{16}(P_{sm} - P_{ca})\right) \tag{6}$$

where the cathode pressure is:

$$P_{ca} = P_{O_2} + P_{N_2} + \gamma_2 \tag{7}$$

$$\Psi = \left(\frac{P_{sm}}{\gamma_{11}}\right)^{\gamma_{12}} - 1 \tag{8}$$

and the compressor mass flow rate is assumed proportional to the compressor rotational speed:

$$W_{cp} = \gamma_{17}\omega_{cp} \quad (9)$$

This approximation corresponds to a local linear approximation of the compressor characteristic map around the nominal operating point, as commonly adopted in PEMFC air supply system models. The control input is the compressor motor voltage V_{cm}, and the stack current I_{st} acts as a measurable disturbance. The cathode outlet mass flow rate $W_{ca,out}$ is determined using the standard nozzle equation [28]:

$$W_{ca,out} = k_{ca,out}\,(P_{sm} - P_{ca}) \quad (10)$$

where, $k_{ca,out}$ denotes the cathode outlet orifice coefficient. The pressure $P_{ca} = y_2$ is directly measured; therefore, $W_{ca,out}$ can be expressed as a known function of measurable signals. The parameters $\gamma_1, \ldots, \gamma_{19}$ are derived from the physical constants listed in Tables 1 and 2.

Table 1. Derived constants for state-space model

Constant	Expression
γ_1	$RT_{f_c}\,k_{ca,in}\,x_{O_2,atm} \,/\, (M_{O_2}\,V_{ca}(1 + W_{ca,in}))$
γ_2	P_{sat}
γ_3	$RT_{f_c} \,/\, V_{ca}$
γ_4	$1/M_{O_2}$
γ_5	$1/M_{N_2}$
γ_6	$M_v\,P_{sat} \,/\, M_a$
γ_7	$nRT_{f_c} \,/\, (4FV_{ca})$
γ_8	$RT_{f_c}k_{\mathrm{ca,in}}(1 - \mathrm{x}_{O_2,\mathrm{atm}}) \,/\, (\mathrm{M}_{\mathrm{N2}}\,V_{ca}(1 + \omega_{\mathrm{atm}}))$
γ_9	$f \,/\, J_{cp}$
γ_{10}	$C_pT_{atm} \,/\, (\eta_{cp}\,J_{cp})$
γ_{11}	P_{atm}
γ_{12}	$(\gamma_r - 1)/\gamma_r$
γ_{13}	$\eta_{cm}\,k_t \,/\, (J_{cp}\,R_{cm})$
γ_{14}	$RT_{atm} \,/\, (M_a\,V_{sm})$
γ_{15}	$1/\eta_{cp}$
γ_{16}	$\mathrm{k}_{\mathrm{ca,in}}$
γ_{17}	$\eta_v\,\rho_a\,V_{cp,r}/t_r \,/\, (2\pi)$
γ_{18}	$k_{ca,in}\,x_{O_2,atm} \,/\, (1 + W_{ca,in})$
γ_{19}	$n\,M_{O_2} \,/\, (4F)$

2.3 Measured outputs

The output vector available for fault diagnosis consists of four measurable signals:

$$y = [y_1\ y_2\ y_3\ y_4]^{\mathrm{T}} = [W_{cp}\ P_{ca}\ \omega_{cp}\ P_{sm}]^{\mathrm{T}} \quad (11)$$

where, y_1 is the compressor mass flow rate (mass air flow sensor), y_2 is the cathode pressure, y_3 is the compressor angular velocity (tachometer), and y_4 is the supply manifold pressure (pressure sensor).

Table 2. Physical parameters of the proton exchange membrane fuel cell (PEMFC) air supply system

Parameter	Symbol	Value /Unit
Number of cells	n	381
Specific heat ratio	γ_{r}	1.4
Gas constant	R	8.314 J/(mol K)
Faraday constant	F	96485 C/mol
Atmospheric pressure	P_{atm}	101325 Pa
FC temperature	T_{f_c}	353.15 K
Ambient temperature	T_{atm}	298.15 K
Specific heat of air	C_p	1004 J/(kg K)
O_2 molar fraction	$x_{O_2,atm}$	0.23
Molar mass of air	M_{a}	28.97 g/mol
Molar mass of O_2	M_{O_2}	32.0 g/mol
Molar mass of N_2	M_{N_2}	28.0 g/mol
Molar mass of H_2O	M_v	18.0 g/mol
Cathode volume	V_{ca}	0.01 m³
Manifold volume	V_{sm}	0.02 m³
Compressor inertia	J_{cp}	5×10^{-5} kg m²
Compressor efficiency	η_{cp}	0.80
Motor efficiency	η_{cm}	0.98
Motor torque constant	k_t	0.0153 Nm/A
Motor back-EMF const.	k_v	0.0153 V s/rad
Motor resistance	R_{cm}	0.82 Ω
Manifold outlet coeff.	$k_{sm,out}$	3.629×10^{-5} kg/(Pa s)
Cathode inlet coeff.	$k_{ca,in} = k_{sm,out}$	3.629×10^{-5} kg/(Pa s)
Cathode outlet coeff.	$k_{ca,out}$	0.76×10^{-4}
Air density	ρ_a	1.23 kg/m³
Compressor displ.	$V_{cp,r}/t_r$	5×10^{-4} m³/rev
Motor friction	f	0.00136 Nm s/rad

Note: EMF = Electro Motive Force

2.4 Fault modeling

Two categories of faults affecting the air supply subsystem are considered.

2.4.1 Actuator fault (compressor motor degradation)

Increased friction in the compressor motor bearings or winding resistance changes are modeled as a multiplicative variation in the back-electromotive force (back-EMF) constant, where $\theta_a(t)$ (the actuator fault) represents the relative fault magnitude, with $\theta_a = 0$ corresponding to nominal operation. The faulty compressor dynamics become:

$$\dot{\omega}_{cp} = -\gamma_9\omega_{cp} - (\gamma_{10}/\omega_{cp})\Psi W_{cp} + \gamma_{13}V_{cm} - (k_v + \Delta k_v)\omega_{cp} \quad (12)$$

where,

$$\theta_a(t) = \Delta k_v \quad (13)$$

2.4.2 Process fault (supply manifold leakage)

In the existing literature, leakage from the supply manifold has been treated in several different ways. Escobet et al. [29] proposed a model-based diagnosis scheme in which the leakage was represented through a modification of the constant γ_{16} (physically linked to the outlet flow coefficient $k_{sm,out}$). Similar formulations were later adopted by de Lira et al. [30] within LPV observer frameworks for PEMFC fault detection and isolation. Laghrouche et al. [31] also worked on related airfeed fault reconstruction using adaptive second-order sliding mode observers. Treating the leak as an artificial enlargement of the cathode inlet orifice tends to mix the leak flow with the normal discharge flow, which can mask the fault during transients.

A physically consistent description, following the classical nozzle equation, models the leakage as an additional mass flow that depends explicitly on the pressure difference between the manifold and the atmosphere. The fault signal θ_p (t) (the process fault) is introduced as an additive term of loss of mass-flow in the supply manifold pressure dynamics:

$$\theta_p\,(\mathrm{t}) = W_{loss} \tag{14}$$

$$W_{loss} = k_{smf}(P_{sm} - P_{atm}) \tag{15}$$

$$\dot{P}_{sm} = \gamma_{14}[1 + \gamma_{15}\Psi](W_{cp} - \gamma_{16}(P_{sm} - P_{ca}) - \theta_p) \tag{16}$$

The value of k_{smf} represents the intensity of the fault. Tables 1 and 2 list the derived constants and physical parameters used in the model.

3. ALGEBRAIC OBSERVABILITY AND DIRECT FAULT RECONSTRUCTION

3.1 Algebraic observability framework

A nonlinear system is algebraically observable [30, 31]

$$\dot{x} = f(x,u), y = h(x) \tag{17}$$

If there exist finite positive integers μ and ν such that $x(t) = \Phi(y, \dot{y}, \ldots, y(\mu), u, \dot{u}, \ldots, u(\nu))$, where $\Phi(\cdot)$ is a (possibly nonlinear) vector-valued function. In other words, each state component can be written as a function of measurable quantities and their derivatives.

3.2 Direct signal recovery from measured outputs

The algebraic reconstructibility of the signals required for fault diagnosis in the PEMFC air supply system is established using only the measured output vector Eq. (11) and known inputs V_{cm}, I_{st}.

Step 1: Compressor speed and manifold pressure. The outputs y_3 and y_4 provide two signals directly: $\omega_{cp} = y_3$, $P_{sm} = y_4$.

Step 2: Sum of cathode partial pressures. From the definition of P_{ca} and the output $y_2 = P_{ca}$, $P_{O_2} + P_{N_2} = y_2 - \gamma_2$. Thus, the sum of partial pressures is directly measurable at every instant.

It is worth noting that recovering the individual partial pressures P_{O_2} and p_{N_2} separately is not required for fault reconstruction. The actuator fault formula depends only on y_3 , y_4 ,V_{cm}, while the process fault formula depends only on y_1 , y_2 and y_4. The full output vector therefore provides all information necessary for fault diagnosis without any additional simplifying assumptions on the cathode gas composition.

3.3 Actuator fault reconstruction

The fault reconstruction Eq. (18) uses a part of the model that is independent of the rest. Consider the compressor dynamics with the actuator fault. Since $y_3 = \omega_{cp}$ is directly measured, we can differentiate y_3 with respect to time to obtain:

$$\dot{y}_3 = \Theta_1(y_3, y_4, u) + \Omega_1(y_3)\theta_a(t) \tag{18}$$

where,

$$\Theta_1(y_3, y_4, u) = -\gamma_9 y_3 - \gamma_{10}\gamma_{17}\Psi + \gamma_{13}V_{cm} - \gamma_{13}k_v y_3 \tag{19}$$

$$\Omega_1(y_3) = -\gamma_{13}y_3 \tag{20}$$

Both Θ_1 and Ω_1 depend on the measurable signals y_3, y_4, and the known input V_{cm}. Solving for the actuator fault:

$$\hat{\theta}_a(t) = \frac{(\dot{y}_3 - \Theta_1(y_3, y_4, u))}{\Omega_1(y_3)} \tag{21}$$

3.4 Process fault reconstruction

Similarly, for the supply manifold dynamics with leakage, since $y_4 = P_{sm}$ is measured:

$$\dot{y}_4 = \Theta_2(y_1, y_2, y_4) + \Omega_1(y_2, y_4)\theta_p \tag{22}$$

where,

$$\Theta_2(y_1, y_2, y_4) = \gamma_{14}[1 + \gamma_{15}\Psi](y_1 - \gamma_{16}(y_4 - y_2)) \tag{23}$$

$$\Omega_1(y_2, y_4) = -\gamma_{14}[1 + \gamma_{15}\Psi] \tag{24}$$

with $\Psi = (y_4/\gamma_{11})\hat{}\gamma_{12} - 1$. All quantities are expressed through the measured outputs y_1 , y_2 , y_4 only. The process fault reconstruction is:

$$\hat{\theta}_p(t) = \frac{(\dot{y}_4 - \Theta_2(y_1, y_2, y_4))}{\Omega_1(y_2, y_4)} \tag{25}$$

The actuator fault Eq. (21) depends only on y_3 , y_4 ,V_{cm}, and $\dot{y}_3$, while the process fault Eq. (25) depends only on y_1 , y_2 , y_4 and $\dot{y}_4$. The two reconstruction expressions are therefore structurally decoupled in the sense that each fault is recovered from a distinct subset of measurements and a distinct output derivative. However, the underlying PEMFC dynamics are physically coupled: the compressor drives the manifold pressure, and the manifold pressure influences the cathode, which in turn affects the compressor load. Consequently, while the reconstruction formulas are algebraically independent, dynamic coupling interactions between the fault estimates may still produce transient errors during rapid

operating-point transitions or simultaneous fault occurrences.

The fault reconstruction formulas involve a division by the sensitivity terms $\Omega_1(y_3)$ and $\Omega_2(y_2, y_4)$, respectively. For Eq. (21), Ω_1 becomes zero only if the compressor speed $y_3 = 0$, which is outside any realistic operating regime. For Eq. (25), Ω_2 reaches zero when $y_2 = y_4$ (zero pressure gradient across the manifold), which cannot occur under normal or faulty operating conditions since the compressor ensures a positive pressure differential.

4. ROBUST EXACT DIFFERENTIATOR FOR DERIVATIVE ESTIMATION

The algebraic reconstruction Eqs. (21) and (25) require real-time estimates of $\dot{y}_3$ and $\dot{y}_4$. Standard numerical differentiation based on finite differences is well known to amplify high-frequency measurement noise and is therefore unsuitable for real-time implementation. To overcome this limitation, the technique of robust exact differentiation, originally proposed by Levant [28, 29] is employed. This class of differentiators achieves exact estimation of the first-order time derivative of a measured signal in finite-time, provided that the second derivative of the signal is uniformly bounded.

The robust exact differentiator for the signal y_i is defined by the following second-order dynamical system [28]:

$$\zeta_{i,1} = -\lambda L_i^{1/2} |\zeta_{i,1} - y_i|^{1/2} sign(\zeta_{i,1} - y_i) + \zeta_{i,2} \quad (26)$$

$$\zeta_{i,2} = -\alpha L_i sign(\zeta_{i,1} - y_i) \quad (27)$$

Two instances of the differentiator Eqs. (26) and (27) are implemented in parallel, one for each fault channel. The first is applied to $y_3 = \omega_{cp}$, providing the estimate $\widehat{\dot{y}_3} = \zeta_{3,2}$ required in the actuator fault reconstruction expression Eq. (21). The second is applied to $y_4 = P_{sm}$, yielding $\widehat{\dot{y}_4} = \zeta_{4,2}$ for the process fault reconstruction expression Eq. (25).

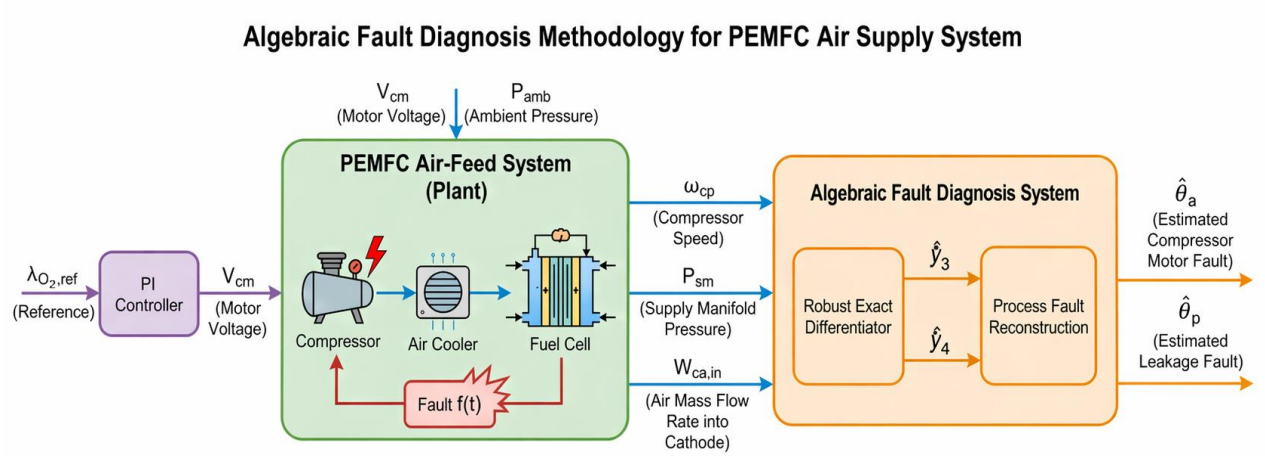

Figure 2. Algebraic fault diagnosis and reconstruction architecture for proton exchange membrane fuel cell (PEMFC) air-feed system

The parameters $\lambda = 1.0$ and $\alpha = 1.1$ are kept fixed as in studies [28, 32], so that the only tuning parameter is the channel-dependent bound L_i, which must satisfy:

$$L_i \geq |\ddot{y}_i(t)| \quad t \geq 0 \quad (28)$$

The bound L_i is determined offline by numerically evaluating the second derivative of each output signal over the expected operating range from the Pukrushpan model.

When the inequality in Eq. (28) is satisfied, the estimation errors converge to zero in finite-time [28], ensuring exact reconstruction of the fault magnitudes using Eqs. (21) and (25).

The complete fault diagnosis architecture, illustrating the signal flow from the PEMFC plant measurements through the robust exact differentiators to the algebraic fault reconstruction blocks, is summarized in Figure 2. Figure 3 presents the detailed implementation flowchart of the proposed scheme, showing how the measured outputs y_3 and y_4 are processed through robust exact differentiators and algebraic reconstruction blocks to obtain the fault estimates $\hat{\theta}_a(t)$ and $\hat{\theta}_p(t)$.

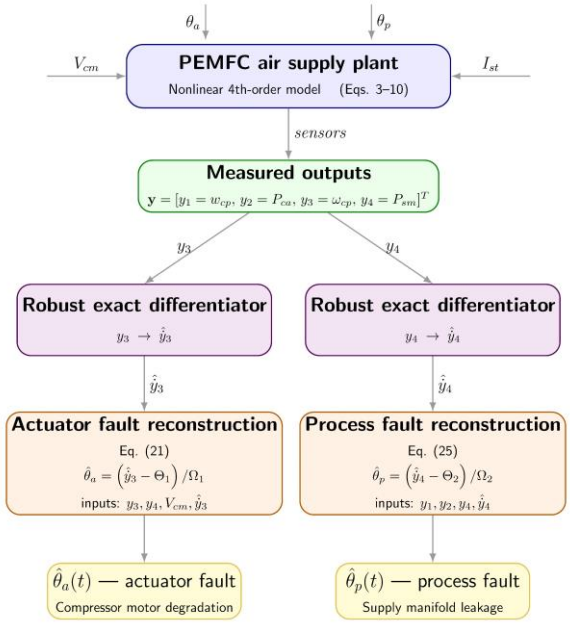

Figure 3. Implementation flowchart of the proposed algebraic fault diagnosis scheme

Table 3. Simulation environment and software specifications, central processing unit (CPU), random access memory (RAM), operating system (OS)

Item	Specification
CPU	Intel Core i5-6300U @ 2.40 GHz
RAM	8 GB DDR4
OS	Windows 10
Software	MATLAB R2018a / Simulink
Solver	ode45, fixed step 0.001 s
Simulation time	213.80 seconds (3.56 minutes)
Noise	Band-limited white noise (seeds and power noise varied)

5. SIMULATION RESULTS

The proposed fault diagnosis framework is validated on the nonlinear Pukrushpan PEMFC model [27], implemented in MATLAB/Simulink with the parameters of Tables 1 and 2. The simulation environment and software specifications are summarized in Table 3. A proportional-integral (PI) controller regulates the oxygen excess ratio λ_{O_2} to its reference value of 2 by adjusting the compressor motor voltage V_{cm}. The stack current I_{st} follows a step-wise profile from 150 A to 300 A over a 30-second window, as shown in Figure 4.

Two fault scenarios are considered: an actuator fault θ_a (compressor motor degradation) modelled as a 30% reduction in the back-EMF constant from $t = 8$ s to $t = 14$ s, followed by a 60% reduction from $t = 14$ s to $t = 22$ s; and a process fault θ_p (supply manifold leakage) modelled as a 20% increase in the cathode inlet orifice coefficient from $t = 6$ s to $t = 12$ s, followed by a 50% increase from $t = 12$ s to $t = 20$ s. Introduced simultaneously to assess the decoupled reconstruction capability of the scheme.

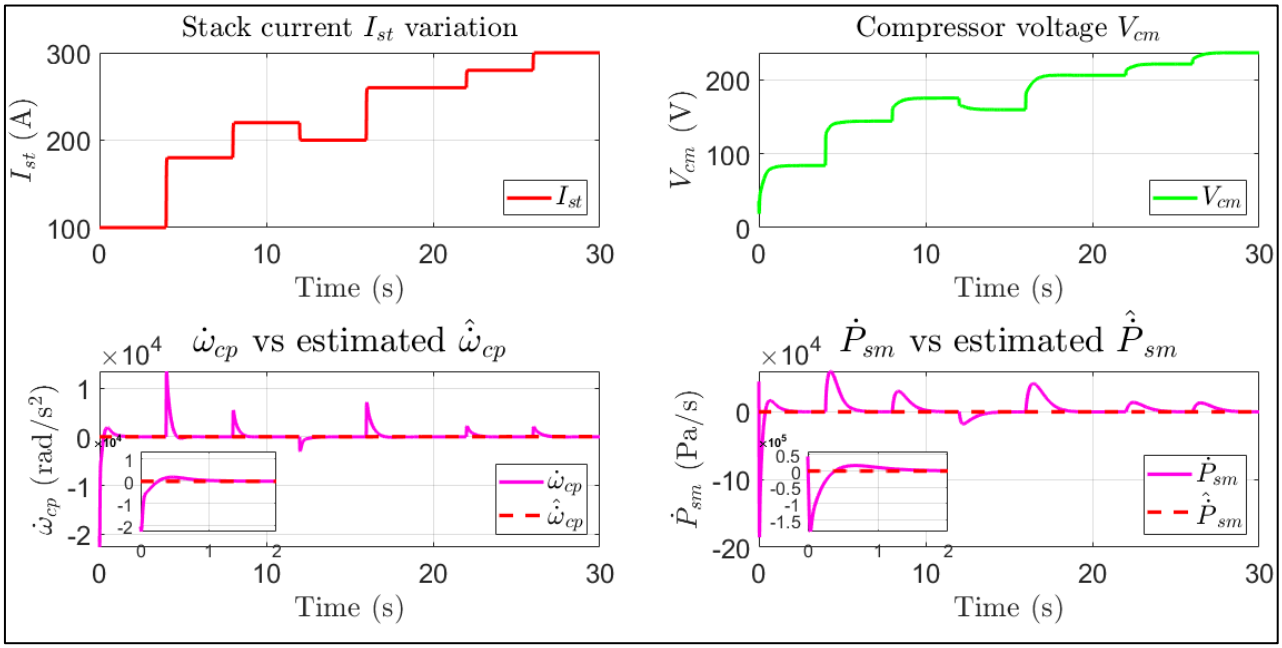

Figure 4. System inputs, control signal, and derivative estimation performance

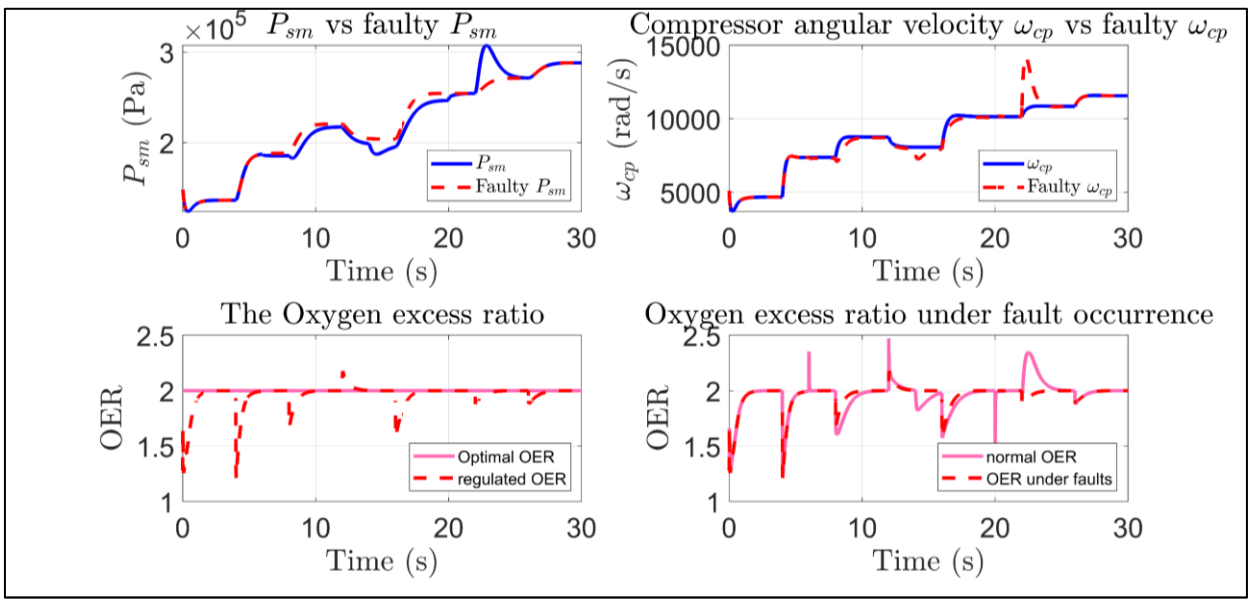

Figure 5. Physical system behavior under fault conditions

Figure 4 also shows the derivative estimation performance of the two differentiators. Brief transient peaks appear at each load step, which is consistent with the abrupt changes imposed on the system. These errors decay rapidly, and accurate tracking of both $\dot{\omega}_{cp}$ and $\dot{P}_{sm}$ is achieved within approximately 2 seconds, in agreement with the finite-time convergence.

The physical effect of the faults on system behavior is illustrated in Figure 5. The manifold pressure and compressor speed deviate from their nominal trajectories once the faults are active. As a consequence, the oxygen excess ratio drops noticeably during load transients, indicating that undetected faults directly compromise cathode oxygen supply and fuel cell efficiency.

The air leakage fault θ_p is reconstructed as shown in Figure 6. The estimated signal $\hat{\theta}_p$ faithfully tracks the ramp reference after a short initial transient of approximately 1 to 2 seconds. The brief spikes at current step instants are due to the differentiator reconvergence interval and do not affect the steady-state reconstruction accuracy.

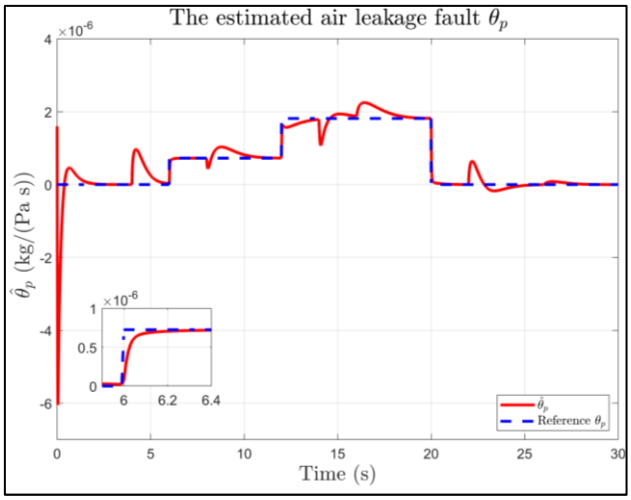

Figure 6. Air leakage fault $\hat{\theta}_p$ reconstruction

The motor fault θ_a is reconstructed as shown in Figure 7. The estimated signal $\hat{\theta}_a$ follows the fault scenario with high fidelity. The proposed scheme is capable of reconstructing both actuator and process fault signals simultaneously and accurately in the presence of load variation, without requiring threshold tuning or asymptotic observer convergence.

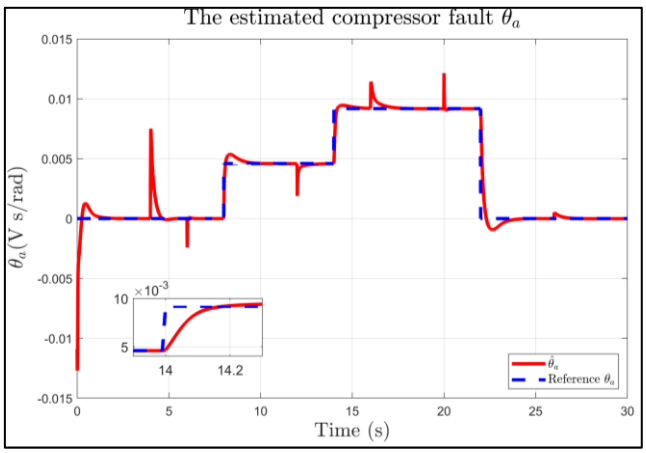

Figure 7. The motor fault reconstruction $\hat{\theta}_a$

5.1 Sensitivity and robustness analysis

To test the robustness of the proposed algebraic observer, simulations were carried out in the presence of measurement noise on $y_3 = \omega_{cp}$ and $y_4 = P_{sm}$. Let $y_{(f_a)} = y_3 + f_a(t)$ be the noisy measurement of y_3 and $y_{(f_p)} = y_4 + f_p(t)$ the noisy measurement of y_4, where f_a and f_p are noisy signals shown in Figure 8. It is possible to see that the algebraic observer estimates both faults well enough in spite of the noise in the measurements.

To quantify robustness, 30 independent runs were performed at a signal to noise ratio (SNR) of 40 dB. The resulting fault estimates were identical across all runs (standard deviation $< 10^{-20}$), because the robust exact differentiator [24] yields exact derivatives in finite-time, making the algebraic reconstruction deterministic. Table 4 summarises the mean settling times, steady state errors, 95% confidence intervals, and root mean square error (RMSE). The zero standard deviation and degenerate confidence intervals reflect the perfect repeatability of the method. For a more severe scenario (SNR = 20 dB), result is shown in Figure 9. Even with this higher noise level, the estimated faults accurately track the true faults, and the absolute errors remain below $1 \times 10^{(-7)}$ bar for the process fault and $4 \times 10^{(-5)}$ V·s/rad for the actuator fault.

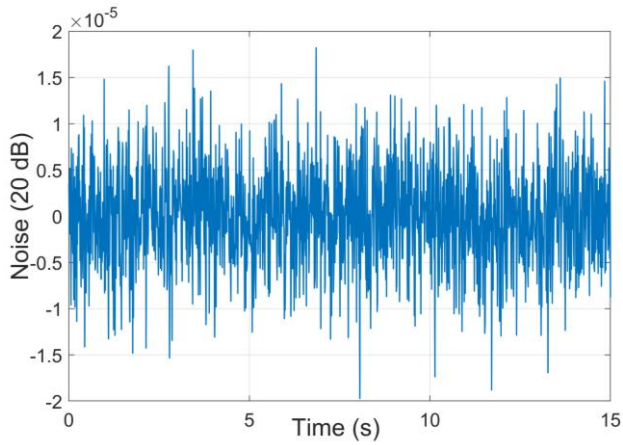

Figure 8. Noise affecting the system outputs (signal to noise ratio, SNR = 20 dB)

Table 4. Statistical performance of fault reconstruction over 30 independent runs (standard deviation (SD), signal to noise ratio (SNR) of 40 dB and root mean square error (RMSE))

Fault	Metric	Mean ± SD	95% Confidence Interval	RMSE (after settling)
θ_p (leakage)	Settling time (s)	0.2600 ± 0.0000	[0.2600, 0.2600]	–
	Steady-state absolute error (bar)	(2.90 ± 0.00) × 10^{-8}	–	(4.15 ± 0.00) × 10^{-8}
θ_a (motor)	Settling time (s)	2.6300 ± 0.0000	[2.6300, 2.6300]	–
	Steady-state absolute error (V·s/rad)	(3.68 ± 0.00) × 10^{-5}	–	(9.08 ± 0.00) × 10^{-5}

The zoomed-in insets (5.9 – 6.2 s) confirm that transients are handled without oscillations. The proposed algebraic observer is highly robust to measurement noise, providing deterministic, finite-time fault reconstruction with negligible steady-state error. To visualise the statistical spread, Figure 10 presents the results under elevated noise (SNR = 20 dB). The shaded area (mean ± 1σ) remains very narrow, demonstrating the method's robustness even under severe measurement noise.

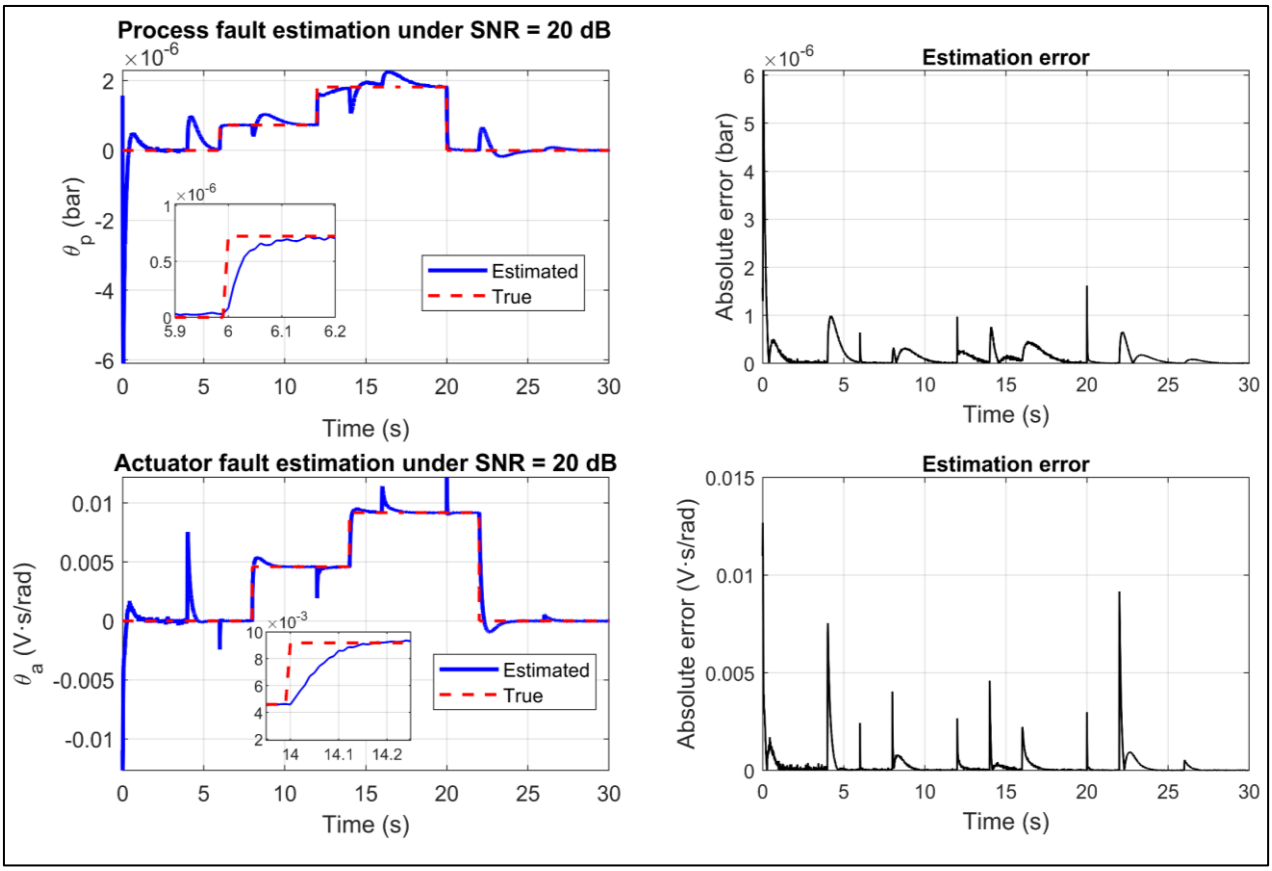

Figure 9. Fault estimation under noise (SNR = 20 dB)

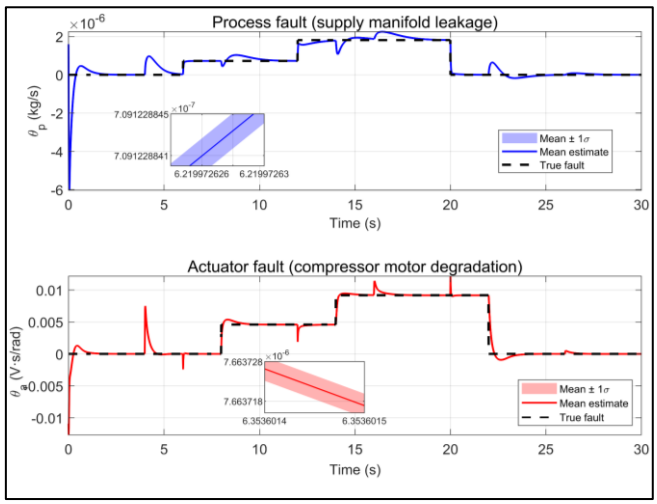

Figure 10. Estimated faults (mean ± 1σ) vs. true faults under measurement noise (SNR = 20 dB)

5.2 Comparison with the super-twisting sliding-mode observer

To further evaluate the proposed scheme, Table 5 compares its performance with a super-twisting sliding-mode observer (ST-SMO) applied to the same PEMFC air-feed system in terms of convergence, simultaneous fault capability, and chattering. The ST-SMO is able to reconstruct the supply manifold leakage fault θ_p when considered alone, with a settling time of approximately 0.4 s (Figure 11). However, it does not allow simultaneous estimation of the actuator fault θ_a, and therefore requires a second observer specifically designed for the compressor dynamics.

Table 5. Comparison of the super-twisting sliding-mode observer (ST-SMO) and proposed algebraic fault reconstruction method

Property	Proposed Algebraic Method	ST-SMO
Faults reconstructed	θ_a and θ_p simultaneously	θ_p only (single fault)
Convergence type	Finite-time	Finite-time
Requires full state observer	No	Yes
Tuning parameters	2 scalars (L_3, L_4)	Gain matrix + switching gains
Settling time $\hat{\theta}_p$	0.1s	0.4 s
Settling time $\hat{\theta}_a$	0.2s	Not reconstructed
Simultaneous fault capability	Yes	No requires second observer
Chattering	None	Present (filtering)

In contrast, the proposed algebraic scheme reconstructs both faults simultaneously in approximately 2 s using two decoupled expressions that do not rely on shared state estimation. This significantly simplifies the design and reduces the tuning effort to only two scalar bounds, L_3 and L_4.

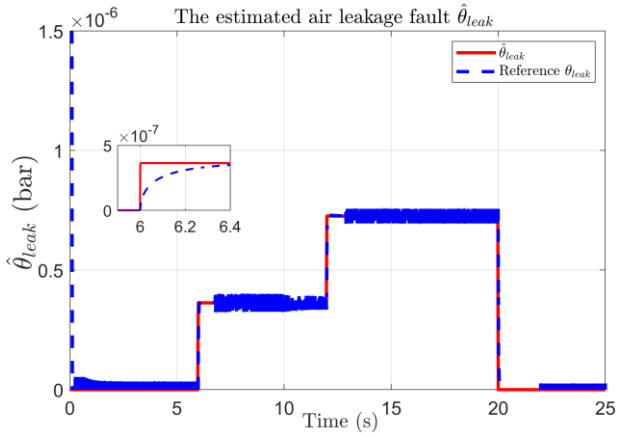

Figure 11. Reconstruction of the supply manifold leakage fault $\hat{\theta}_p$ using the super-twisting sliding-mode observer (ST-SMO)

6. CONCLUSIONS

This paper has developed a finite-time fault reconstruction scheme for the air-feed subsystem of a PEMFC. The approach expresses actuator and process fault magnitudes as direct algebraic functions of the measured outputs and their first derivatives. The required derivatives are supplied by a robust exact differentiator where the second derivative of the measured signal is determined systematically from the physical model, with no residual threshold adjustment needed. Simulation results on the Pukrushpan benchmark, operated under a PI-controlled step current profile, show that both compressor motor degradation and supply manifold leakage are simultaneously reconstructed with a settling time of approximately two seconds and negligible steady-state error across the full load range tested. The two reconstruction channels remain decoupled despite the physical coupling of the underlying PEMFC dynamics. These results support the practical relevance of the method for PEMFC supervision and motivate future experimental validation on a real test bench.

The present study is limited to simulation-based validation using a single-stack PEMFC model; experimental verification on a real test bench is required to confirm practical applicability. Additionally, the algebraic reconstruction formulas are parameter-dependent, meaning that different stack geometries or multi-stack configurations would require re-derivation. Future work will focus on hardware in the loop (HIL) experiments, extension to multi-stack systems, and integration of the fault estimates into a fault-tolerant control strategy.

REFERENCES

[1] Larminie, J., Dicks, A. (2003). Fuel Cell Systems Explained, 2nd ed. John Wiley & Sons, Chichester, UK. https://doi.org/10.1002/9781118878330

[2] Wang, Y., Chen, K.S., Mishler, J., Cho, S.C., Adroher, X.C. (2011). A review of polymer electrolyte membrane fuel cells: Technology, applications, and needs on fundamental research. Applied Energy, 88(4): 981-1007. https://doi.org/10.1016/j.apenergy.2010.09.030

[3] de Bruijn, F.A., Dam, V.A.T., Janssen, G.J.M. (2008). Review: Durability and degradation issues of PEM fuel cell components. Fuel Cells, 8(1): 3-22. https://doi.org/10.1002/fuce.200700053

[4] Zheng, Z., Petrone, R., Pera, M.C., Hissel, D., Becherif, M., Pianese, C., Steiner, N.Y., Sorrentino, M. (2013). A review on non-model based diagnosis methodologies for PEM fuel cell stacks and systems. International Journal of Hydrogen Energy, 38(21): 8914-8926. https://doi.org/10.1016/j.ijhydene.2013.04.007

[5] Lv, Z., Wu, X., Liu, H., Jiang, J., Hou, M. (2023). Diagnosis of PEM fuel cell system based on electrochemical impedance spectroscopy and deep learning method. IEEE Transactions on Industrial Electronics, 70(1): 657-666. https://doi.org/10.1109/TIE.2023.3241404

[6] Chen, Y., Zhang, C., Zhang, Q., Hu, H., Wu, W. (2022). Data-driven flooding fault diagnosis method for proton-exchange membrane fuel cells using deep learning technologies. Journal of Power Sources, 537: 231511. https://doi.org/10.1016/j.enconman.2021.115004

[7] Frank, P.M. (1994). Enhancement of robustness in observer-based fault detection. International Journal of Control, 59(4): 955-981. https://doi.org/10.1080/00207179408923112

[8] Edwards, C., Spurgeon, S.K., Patton, R.J. (2000). Sliding mode observers for fault detection and isolation. Automatica, 36(4): 541-553. https://doi.org/10.1016/S0005-1098(99)00177-6

[9] Chen, J., Patton, R.J. (1999). Robust Model-Based Fault Diagnosis for Dynamic Systems. Kluwer Academic Publishers, Boston, MA, USA. https://doi.org/10.1007/978-1-4615-5149-2

[10] Vepa, R. (2012). Adaptive state estimation of a PEM fuel cell. IEEE Transactions on Energy Conversion, 27(2): 457-467. https://doi.org/10.1109/TEC.2012.2190073

[11] de Lira, S., Puig, V., Quevedo, J., Husar, A. (2011). LPV observer design for PEM fuel cell system: Application to fault detection. Journal of Power Sources, 196(9): 4298-4305. https://doi.org/10.1016/j.jpowsour.2010.11.084

[12] Yang, D., Wang, Y., Chen, Z. (2020). Robust fault diagnosis and fault tolerant control for PEMFC system based on an augmented LPV observer. International Journal of Hydrogen Energy, 45(24): 13508-13522. https://doi.org/10.1016/j.ijhydene.2020.03.063

[13] Guo, X., Fan, N., Dong, Z., Wang, C. (2024). Adaptive prescribed performance control for PEM fuel cell air supply systems with unknown air compressor faults. IEEE Transactions on Industrial Electronics, 71(5): 4575-4585. https://doi.org/10.1109/TIE.2023.3312416

[14] Wang, Z., Guo, X., Dong, Z., Fan, N., Cao, S. (2024). Fixed time adaptive fault tolerant sliding mode control of PEMFC air supply system. International Journal of Hydrogen Energy, 55: 1434-1444. https://doi.org/10.1016/j.ijhydene.2023.11.264

[15] Wang, Z., Guo, X., Dong, Z., Fan, N., Cao, S. (2024). Finite-time sliding mode fault-tolerant control of PEM fuel cell air supply system. Asian Journal of Control, 26(6): 3014-3026. https://doi.org/10.1002/asjc.3376

[16] Diop, S., Fliess, M. (1991). Nonlinear observability,

identifiability, and persistent trajectories. In: Proceedings of the 30th IEEE Conference on Decision and Control, Brighton, UK, pp. 714-718. https://doi.org/10.1109/CDC.1991.261405
[17] Fliess, M., Sira-Ramirez, H. (2003). An algebraic framework for linear identification. ESAIM: Control, Optimisation and Calculus of Variations, 9: 151-168. https://doi.org/10.1051/cocv:2003008
[18] Baroud, Z., Benalia, A., Ocampo-Martinez, C. (2016). Algebraic observer design for PEM fuel cell systems. In Proceedings of the 8th International Conference on Modelling, Identification and Control (ICMIC 2016), Algiers, Algeria. https://doi.org/10.1109/ICMIC.2016.7804245
[19] Baroud, Z., Benalia, A., Ocampo-Martinez, C. (2018). Algebraic observer-based output-feedback controller design for a PEM fuel cell air-supply subsystem. IET Renewable Power Generation, 12(13): 1519-1527. https://doi.org/10.1049/iet-rpg.2018.5421
[20] Jing, H., Zhang, C., Zhu, M., Chen, X., Shen, X. (2023). Multi-objective sliding mode control of proton exchange membrane fuel cell systems based on adaptive algebraic observers. Proceedings of the Institution of Mechanical Engineers, Part I: Journal of Systems and Control Engineering, 237(8): 1400-1414. https://doi.org/10.1177/09576509231201995
[21] Liu, J., Luo, W., Yang, X., Wu, L. (2016). Robust model-based fault diagnosis for PEM fuel cell air-feed system. IEEE Transactions on Industrial Electronics, 63(5): 3261-3270. https://doi.org/10.1109/TIE.2016.2535118
[22] Flores-Mendez, J., Moreno, J.A., Luviano-Juárez, A. (2022). Fault diagnosis based on algebraic identification assisted by extended state observers. Nonlinear Dynamics, 107(1): 887-906. https://doi.org/10.1007/s11071-021-07053-3
[23] Levant, A. (1998). Robust exact differentiation via sliding mode technique. Automatica, 34(3): 379-384. https://doi.org/10.1016/S0005-1098(97)00209-4
[24] Levant, A. (2003). Higher-order sliding modes, differentiation and output-feedback control. International Journal of Control, 76(9-10): 924-941. https://doi.org/10.1080/0020717031000099029
[25] Moreno, J.A., Osorio, M. (2012). Strict Lyapunov functions for the super-twisting algorithm. IEEE Transactions on Automatic Control, 57(4): 1035-1040. https://doi.org/10.1109/TAC.2012.2186179
[26] Talj, R.J., Hissel, D., Ortega, R., Becherif, M., Hilairet, M. (2010). Experimental validation of a PEM fuel-cell reduced-order model and a motocompressor higher order sliding-mode control. IEEE Transactions on Industrial Electronics, 57(6): 1906-1913. https://doi.org/10.1109/TIE.2009.2029588
[27] Pukrushpan, J.T., Stefanopoulou, A.G., Peng, H. (2004). Control of fuel cell breathing: Initial results on the oxygen starvation problem. IEEE Control Systems Magazine, 24(2): 30-46. https://doi.org/10.1109/MCS.2004.1275430
[28] Pukrushpan, J.T. (2003). Modeling and control of fuel cell systems and fuel processors. Ph.D. Dissertation, University of Michigan, Ann Arbor, MI, USA.
[29] Escobet, T., Feroldi, D., de Lira, S., Puig, V., Quevedo, J., Riera, J., Serra, M. (2009). Model-based fault diagnosis in PEM fuel cell systems. Journal of Power Sources, 192(1): 216-223. https://doi.org/10.1016/j.jpowsour.2008.12.014
[30] de Lira, S., Puig, V., Quevedo, J. (2012). Fault detection and isolation of a real PEM fuel cell using interval LPV observers. In Proceedings of the 8th IFAC Symposium on Fault Detection, Supervision and Safety of Technical Processes (SAFEPROCESS 2012), Mexico City, Mexico, 45(20): 90-95. https://doi.org/10.3182/20120829-3-MX-2028.00171
[31] Laghrouche, S., Liu, J., Ahmed, F.S., Harmouche, M., Wack, M. (2015). Adaptive second-order sliding mode observer-based fault reconstruction for PEM fuel cell air-feed system. IEEE Transactions on Control Systems Technology, 23(3): 1098-1109. https://doi.org/10.1109/TCST.2014.2361869
[32] Shtessel, Y., Edwards, C., Fridman, L., Levant, A. (2014). Sliding Mode Control and Observation. Birkhäuser, New York, NY, USA. https://doi.org/10.1007/978-0-8176-4893-0

NOMENCLATURE

P_{O_2}	oxygen partial pressure in cathode
P_{N_2}	nitrogen partial pressure in cathode
P_{sm}	supply manifold pressure
V_{cm}	compressor motor voltage (control input)
I_{st}	stack current (measurable disturbance)
P_{ca}	cathode total pressure
W_{cp}	compressor mass flow rate
L_i	upper bound for channel i
L_3	bound for $y_3 = \omega_{cp}$
L_4	bound for $y_4 = p_{sm}$

Greek symbols

ω_{cp}	compressor angular velocity
λ_{O_2}	oxygen excess ratio
γ_1 to γ_{19}	derived model constants (see Table 1 for expressions)
Ψ	compressor pressure ratio: $\left(\frac{P_{sm}}{P_{\text{atm}}}\right)^{\frac{\gamma_r-1}{\gamma_r}} - 1$
$\theta_a(t)$	actuator fault: motor degradation (Δk_v)
$\theta_p(t)$	process fault: manifold leakage (W_{loss})
$\Theta_1(y_3, y_4, u)$	measurable function (actuator channel)
$\Theta_2(y_1, y_2, y_4)$	measurable function (process channel)
$\Omega_1(y_3)$	sensitivity term, actuator channel ($-\gamma_{13} y_3$)
$\Omega_2(y_2, y_4)$	sensitivity term, process channel ($-\gamma_{14}[1 + \gamma_{15}\Psi]$)
$\zeta_{i,1}$	1st differentiator state, channel i (estimate of y_i)
$\zeta_{i,2}$	2nd differentiator state, channel i (estimate of dy_i/dt)
α	differentiator gain (fixed: $\alpha = 1.1$)
λ	differentiator gain (fixed: $\lambda = 1.0$)
γ_r	specific heat ratio of air

Subscripts

O_2	oxygen
N_2	nitrogen
sm	supply manifold

cm	compressor motor
st	stack
ca	cathode
cp	compressor
atm	atmospheric
r	ratio
a	actuator
p	process
i	channel index
out	output
in	input

Abbreviations

PEMFC	Proton Exchange Membrane Fuel Cell
EIS	Electrochemical Impedance Spectroscopy
LPV	Linear Parameter-Varying
HOSM	Higher Order Sliding Mode
CPU	Central Processing Unit
RAM	Random Access Memory
OS	Operating System
EMF	ElectroMotive Force
PI	Proportional Integral (controller)
SNR	Signal to Noise Ratio
RMSE	Root Mean Square Error
SD	Standard Deviation
SMO	Sliding Mode Observer
ST-SMO	Super Twisting Sliding Mode Observer
HIL	Hardware in the Loop